nature microbiology

ARTICLES

https://doi.org/10.1038/s41564-018-0289-1

Pulmonary phagocyte-derived NPY controls the pathology of severe influenza virus infection

Seiki Fujiwara[1,16], Midori Hoshizaki[1,16], Yu Ichida[1], Dennis Lex[2], Etsushi Kuroda[3,4], Ken J. Ishii[3,4], Shigeyuki Magi[5], Mariko Okada[5,6], Hiroyuki Takao[1], Masahiro Gandou[1], Hirotaka Imai[1], Ryujiro Hara[1], Herbert Herzog[7], Akihiko Yoshimura[8], Hitoshi Okamura[9], Josef M. Penninger[10,11], Arthur S. Slutsky[12,13], Stefan Uhlig[2], Keiji Kuba[14] and Yumiko Imai[1,15]*

Crosstalk between the autonomic nervous system and the immune system by means of the sympathetic and parasympathetic pathways is a critical process in host defence. Activation of the sympathetic nervous system results in the release of catecholamines as well as neuropeptide Y (NPY). Here, we investigated whether phagocytes are capable of the de novo production of NPY, as has been described for catecholamines. We show that the synthesis of NPY and its Y1 receptor (Y1R) is increased in phagocytes in lungs following severe influenza virus infection. The genetic deletion of *Npy* or *Y1r* specifically in phagocytes greatly improves the pathology of severe influenza virus infection, which is characterized by excessive virus replication and pulmonary inflammation. Mechanistically, it is the induction of suppressor of cytokine signalling 3 (SOCS3) via NPY-Y1R activation that is responsible for impaired antiviral response and promoting pro-inflammatory cytokine production, thereby enhancing the pathology of influenza virus infection. Thus, direct regulation of the NPY-Y1R-SOCS3 pathway on phagocytes may act as a fine-tuner of an innate immune response to virus infection, which could be a therapeutic target for lethal influenza virus infection.

Influenza A viruses have caused worldwide epidemics and pandemics and are a major cause of morbidity and mortality, especially in patients with risk factors such as obesity, diabetes and asthma[1]. In addition, highly pathogenic influenza viruses (that is, avian H5N1 virus) cause severe infection in humans, with mortality rates of up to 60%[2]. Severe influenza virus infections are characterized by extremely high cytokine production and virus replication[2]. However, to date, no effective therapeutics have been developed for the treatment of severe influenza virus infection.

Crosstalk between the autonomic nervous system and the immune system is considered an important biological process in health and disease[3,4]. Activation of the sympathetic nervous system (SNS) by diverse stimuli results in the release of catecholamines, leading to upregulation of the immune system. In addition to SNS-derived neural catecholamines, the de novo synthesis of catecholamines on phagocytes has been shown to enhance acute inflammatory responses[5]. The SNS-derived neuropeptide Y (NPY) is also commonly present in sympathetic nerve terminals and released following SNS stimulation[6], and has been shown to modulate immune function through its specific Y receptors (that is, Y1, Y2, Y4 and Y5) expressed on immune cells[7–9]. However, it is unknown whether any non-neural sources of NPY can contribute to disease pathogenesis. The suppressor of cytokine signalling (SOCS) proteins generally act as negative feedback regulators, minimizing the overproduction of cytokines and downregulating their signalling; however, they can also act as positive regulators, enhancing cytokine production[10–13]. SOCS3 expression is upregulated in lungs infected with the highly pathogenic H5N1 influenza virus[14], and inhibitors of SOCS1 and SOCS3 have been shown to improve the pathology of lethal influenza virus infection[15].

In the present study, we deciphered the underlying mechanisms by which non-neural NPY and Y1R on phagocytes may modulate the SOCS3-mediated antiviral and pro-inflammatory responses[10–13] to severe influenza virus infection, which could potentially be a therapeutic approach.

Results

NPY synthesis is enhanced in pulmonary phagocytes following influenza virus infection in mice. While the role of SNS-derived NPY in controlling immune function has been previously established, only a few studies have focused on the role of non-neural NPY in the regulation of immune cell function[7]. We therefore investigated the function of non-neural NPY in the pathogenesis of severe influenza virus infection. Both mRNA (Fig. 1a) and

[1]Laboratory of Regulation for Intractable Infectious Diseases, Center for Vaccine and Adjuvant Research (CVAR), National Institutes of Biomedical Innovation Health and Nutrition (NIBIOHN), Osaka, Japan. [2]Institute of Pharmacology and Toxicology, Medical Faculty, RWTH Aachen University, Aachen, Germany. [3]Laboratory of Adjuvant Innovation, Center for Vaccine and Adjuvant Research (CVAR), National Institutes of Biomedical Innovation Health and Nutrition (NIBIOHN), Osaka, Japan. [4]Laboratory of Vaccine Science, World Premier International Immunology Frontier Research Center, Osaka, Japan. [5]Laboratory of Cell Systems, Institute for Protein Research, Osaka University, Osaka, Japan. [6]Laboratory for Integrated Cellular Systems, RIKEN Center for Integrative Medical Sciences, Kanagawa, Japan. [7]Neuroscience Division, Garvan Institute of Medical Research, Sydney, New South Wales, Australia. [8]Department of Microbiology and Immunology, Keio University School of Medicine, Tokyo, Japan. [9]Laboratory of Molecular Brain Science, Graduate School of Pharmaceutical Sciences, Kyoto University, Kyoto, Japan. [10]Institute of Molecular Biotechnology in the Austrian Academy of Sciences, Vienna, Austria. [11]Life Science Institute, University of British Columbia, Vancouver, Canada. [12]Keenan Research Center, Li Ka Shing Knowledge Institute, St. Michael's Hospital, Toronto, Ontario, Canada. [13]Interdepartmental Division of Critical Care Medicine, University of Toronto, Toronto, Ontario, Canada. [14]Department of Biochemistry and Metabolic Science, Akita University Graduate School of Medicine, Akita, Japan. [15]Laboratory of Infection Systems, Institute for Protein Research, Osaka University, Osaka, Japan. [16]These authors contributed equally: Seiki Fujiwara, Midori Hoshizaki. *e-mail: y-imai@nibiohn.go.jp

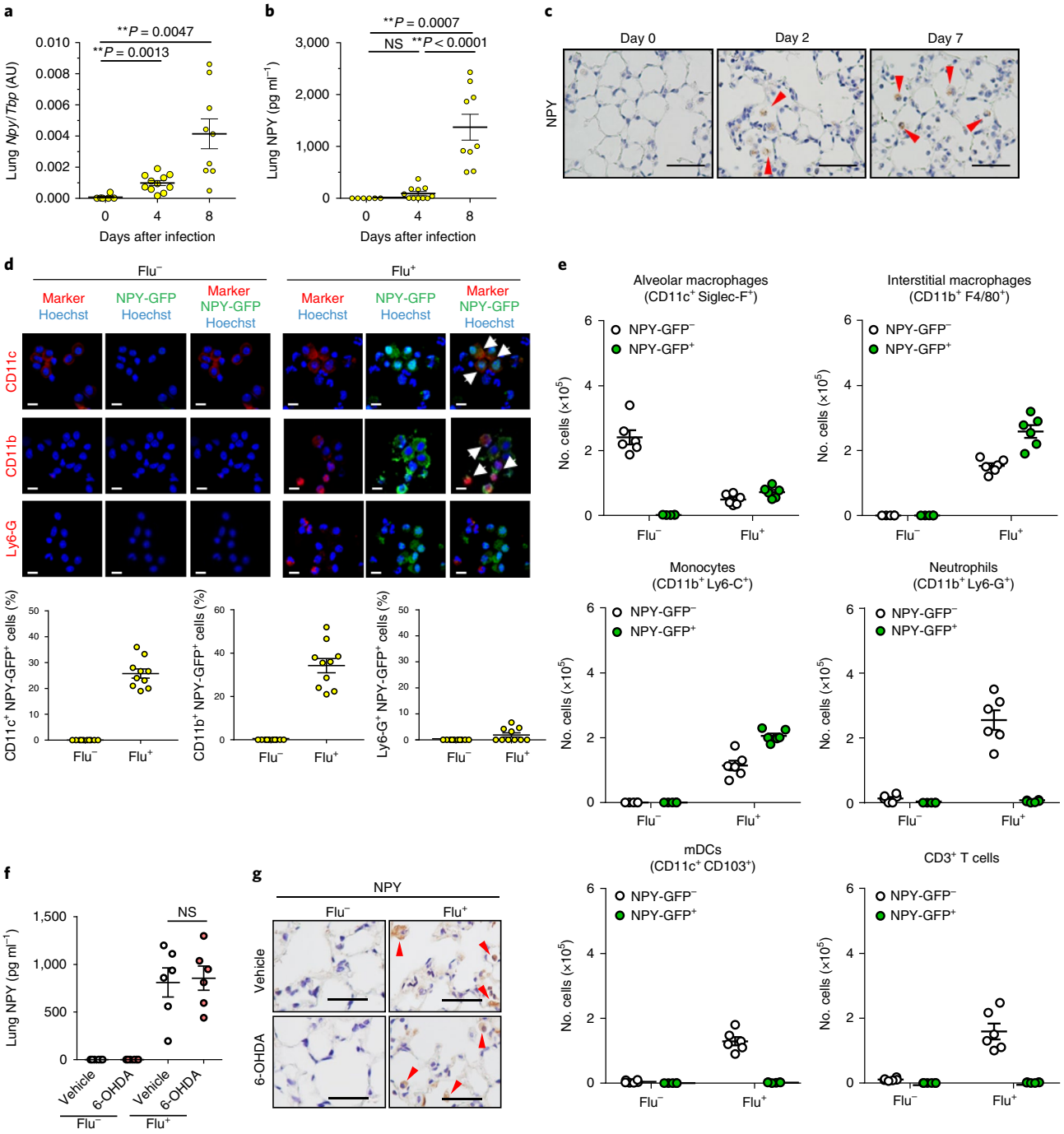

Fig. 1 | NPY is synthesized in excess in pulmonary phagocytes in severe influenza in mice. a,**b**, Wild-type mice were infected with PR8 virus (100 $TCID_{50}$), and lung tissues were obtained at 0, 4 and 8 days after infection. NPY mRNA (**a**) and protein (**b**) levels were then measured ($n = 6$ for day 0, $n = 11$ for day 4 and $n = 9$ for day 8). $^{**}P < 0.01$ between the groups. NS, not significant. One-way ANOVA was used, and if significant, further analysed by two-tailed *t*-tests. **c**,**d**, NPY-GFP mice were infected with PR8 virus (100 $TCID_{50}$). Lung tissue obtained at 0, 2 and 7 days after infection were stained using anti-GFP antibody ($n = 3$ mice per group). Red triangles indicate NGY-GFP+ cells. Representative staining is shown (**c**). BAL fluid was obtained 0 (Flu−) and 5 days (Flu+) post infection, and the cells from the BAL fluids were co-stained with anti-GFP antibody and anti-CD11c, anti-CD11b or anti-Ly6-G antibodies. White arrows show $CD11c^+$ NPY-GFP+ or $CD11b^+$ NPY-GFP+ cells. Representative staining is shown (**d**, upper panel; $n = 3$ mice per group). The images were quantified and the percentage cell numbers of $CD11c^+$ NPY-GFP+, $CD11b^+$ NPY-GFP+, and $Ly6\text{-}G^+$ NPY-GFP+ cells to total cells are shown (**d**, lower panels; $n = 10$ images per group). **e**, NPY-GFP mice were infected with mock or PR8 virus (100 $TCID_{50}$) for 5 days. Cells from the BAL fluids were obtained from mock- (Flu−) or virus-infected (Flu+) mice and subjected to cell counting and flow cytometry analyses. NPY-GFP- or NPY-GFP+ cell numbers of alveolar macrophages, interstitial macrophages, monocytes, neutrophils, mDCs and $CD3^+$ T cells are shown. Data are from six separate experiments. Cell numbers of the NPY+ alveolar macrophages, interstitial macrophages and monocytes were markedly increased following virus infection. **f**,**g**, NPY-GFP mice were subjected to chemical sympathectomy with 6-OHDA and infected with mock or PR8 virus (100 $TCID_{50}$; $n = 6$ mice per group). NPY protein levels (**f**) and NPY-GFP staining (**g**) in lung tissues obtained from mock- (Flu−) and virus-infected (Flu+) mice at 5 days after infection. One-way ANOVA was used. Red triangles show NGY-GFP+ cells. Representative staining is shown **g**. The data in **a**, **b**, **d**, **e** and **f** are presented as the mean ± s.e.m. Scale bars, 50 μm (**c**,**g**), 10 μm (**d**).

protein (Fig. 1b) levels of NPY were significantly increased in the lungs of mice intratracheally infected with influenza virus (A/Puerto Rico/8/34 (H1N1/PR8) strain), in which the lung pathology of this model closely mimics that of severe influenza infection in humans[16,17]. Using NPY-GFP mice that express green fluorescent protein (GFP) under the control of the mouse *Npy* promoter[18], we found that NPY-GFP-positive cells were markedly increased in lungs following influenza virus infection (Fig. 1c). Moreover, these cells appeared to localize to myeloid cells rather than parenchymal cells. To determine the cell types that express NPY in lungs following influenza virus infection, we first examined the expression of NPY in bronchoalveolar lavage (BAL) cells via immunofluorescence. In non-infected lungs, NPY-GFP staining was absent in all cells positive for CD11c, CD11b, Ly6-G, CD103 and CD3 (Fig. 1d; Supplementary Fig. 1a). In contrast, virus-infected lungs showed numerous cells that were positive for both NPY-GFP and CD11c, and NPY-GFP and CD11b (Fig. 1d; Supplementary Fig. 1a). Notably, BAL cells from virus-infected wild-type mice did not show GFP-positive signals (Supplementary Fig. 1b). Next, we performed flow cytometry analysis of the myeloid cells in BAL fluids obtained from non-infected and infected NPY-GFP mice[19–21] (Fig. 1e). The number of NPY-GFP-positive alveolar macrophages ($CD11c^+$ Siglec-F^+), interstitial macrophages ($CD11b^+$ $F4/80^+$) and monocytes (Ly6-C^+ $CD11b^+$) were markedly increased following virus infection (Fig. 1e). Notably, neutrophils (Ly6-G^+ $CD11b^+$), myeloid dendritic cells (mDCs; $CD11c^+$ $CD103^+$), T cells ($CD3^+$) and natural killer (NK) cells ($NK1.1^+$) did not show NPY-GFP signals under non-infected or infected conditions (Fig. 1e; Supplementary Fig. 1c). Together, these data suggest that NPY is mainly expressed in phagocytes, including alveolar and interstitial macrophages and monocytes, in lungs following influenza virus infection.

To identify potential transcription factors, which may be able to initiate *Npy* mRNA expression, we investigated transcription factor-binding motifs nearby the transcriptional start site (TSS) of the *Npy* gene using the CIS-BP database[22], and identified 296 candidate transcription factors. Among them, Jun and JunB were shown to be highly upregulated in our previous microarray analysis of lung tissues after influenza virus infection[16]. Next, RNA sequencing (RNA-seq) of pulmonary phagocytes isolated from non-infected and infected mice was performed. Consistent with our previous data[16], the RNA-seq analysis showed that immediate-early response genes including *Jun*, *JunB* and *Egr1* were upregulated in pulmonary phagocytes following virus infection (Supplementary Fig. 1d).

To exclude the possibility that the elevated NPY levels observed in the virus-infected lungs originated from sympathetic nerve terminals[6], we performed chemical sympathectomy in NPY-GFP mice using 6-hydroxy dopamine (6-OHDA) or reserpine, both of which damage noradrenergic neurons and dopaminergic neurons[23]. Notably, chemical sympathectomy with these chemicals efficiently reduced SNS-derived NPY production (Supplementary Fig. 1e,f). NPY-GFP mice were then intratracheally infected with virus, followed by the administration of vehicle or 6-OHDA. We found that 6-OHDA treatment did not affect the induction of NPY in the virus-infected lungs (Fig. 1f,g). Furthermore, similar to 6-OHDA treatment (Fig. 1f), reserpine treatment did not change the expression of NPY in the virus-infected lungs (Supplementary Fig. 1g). Collectively, our data demonstrate that sympathetic nerves are unlikely to be the sources of NPY.

Deletion of NPY improves the pathology of severe influenza virus infection. Next, we examined whether the expression of NPY actively contributes to the pathology of severe influenza virus infection. Compared with wild-type mice, the survival of infected mice in which NPY was knocked out (NPY-KO) was significantly improved (Fig. 2a,b). Histological analyses also showed that NPY-KO mice had less tissue damage (Fig. 2c), lower lung injury scores (Supplementary Fig. 2a) and less pulmonary oedema formation (Fig. 2d) compared with wild-type mice. Importantly, NPY-KO mice showed less virus replication, as assessed by measuring virus nucleoprotein (NP) mRNA expression (Fig. 2e). Furthermore, the mRNA expression of the pro-inflammatory cytokines *Cxcl1*, *Cxcl2* and interleukin-6 (*Il6*) were lower in NPY-KO than wild-type lungs, while expression of the anti-inflammatory cytokine *Il10* was higher in NPY-KO than wild-type lungs (Fig. 2f; Supplementary Fig. 2b). In addition, a flow cytometry analysis demonstrated that the cell number of phagocytes, including alveolar and interstitial macrophages and monocytes, were significantly decreased in the BAL fluids of virus-infected NPY-KO mice compared with those in wild-type mice (Fig. 2g). By contrast, the cell number of neutrophils, mDCs, T cells and NK cells did not differ between wild-type and NPY-KO mice (Fig. 2g; Supplementary Fig. 2c). These data suggest that deletion of NPY improves the pathology of severe influenza virus infection.

It has been described that PR8 virus can infect macrophages or monocytes[24]. We wondered whether the findings observed in NPY-KO mice were specific for the PR8 virus or whether these findings would also be relevant to other viruses. To test this hypothesis, wild-type and NPY-KO mice were infected with the pandemic H1N1/2009 strain (A/California/04/2009 H1N1), which is known to infect macrophages and monocytes[25]. Again, NPY-KO mice showed improved survival following virus infection (Supplementary Fig. 2d). This result demonstrates that the attenuating phenotype in NPY-KO mice is not only seen for the PR8 virus but also another virus that can infect macrophages and monocytes.

Phagocyte-specific Y1R deletion improves the pathology of influenza virus infection in mice. Y1R and Y2R have been shown to localize to immune cells, including macrophages and neutrophils, with the Y1R being the most abundant[9,26,27]. In the virus-infected lungs Y1R was expressed on cells positive for CD11c, CD11b or Ly6-C, but not on cells positive for Ly6-G, CD103, CD3 or NK1.1 (Fig. 3a; Supplementary Fig. 3a). In addition, compared with non-infected controls, cells double-positive for Y1R and CD11c and Y1R and CD11b were increased in BAL following virus infection (Supplementary Fig. 3b). Thus, similar to NPY, Y1R expression is induced in pulmonary phagocytes positive for CD11c, CD11b or Ly6-C following influenza virus infection.

Next, to examine the function of Y1R on phagocytes, we generated phagocyte-specific Y1R knockout ($Y1R^{PC\text{-}KO}$) mice using M lysozome-Cre mice, which have genes deleted selectively in myeloid cells[28]. Subsequently, wild-type Y1R mice ($Y1R^{PC\text{-}WT}$) and $Y1R^{PC\text{-}KO}$ mice were infected with influenza virus. Notably, Y1Rs were absent in all cells positive for CD11c, CD11b, Ly6-C, Ly6-G, CD103, CD3 or NK1.1 in the $Y1R^{PC\text{-}KO}$ mice (Fig. 3a, right panels). Moreover, lung myeloid cells obtained from $Y1R^{PC\text{-}KO}$ mice demonstrated a loss of Y1R expression (Fig. 3b). These data confirm that Y1R is deleted in pulmonary phagocytes, including macrophages and monocytes, in $Y1R^{PC\text{-}KO}$ mice.

Importantly, compared with wild-type mice, $Y1R^{PC\text{-}KO}$ mice had better survival (Fig. 3c) and lung histology (Fig. 3d). Virus replication (Fig. 3e) and pro-inflammatory cytokine expression (Fig. 3f) in lung tissues were reduced in $Y1R^{PC\text{-}KO}$ compared with $Y1R^{PC\text{-}WT}$ mice. Furthermore, virus titres (Fig. 3g) and IL-6 protein levels (Fig. 3h) in the supernatant of the infected phagocytes were lower in $Y1R^{PC\text{-}KO}$ than $Y1R^{PC\text{-}WT}$ mice. These data indicate that deletion of the Y1R on phagocytes attenuates virus replication and pro-inflammatory cytokine production, resulting in improved pathology of severe influenza virus infection.

Next, to examine whether sympathetic neural NPY is involved in the Y1R-mediated pathology of influenza virus infection, we performed chemical sympathectomy in $Y1R^{PC\text{-}WT}$ and $Y1R^{PC\text{-}KO}$ mice, before infection of the mice with virus with different virus titres.

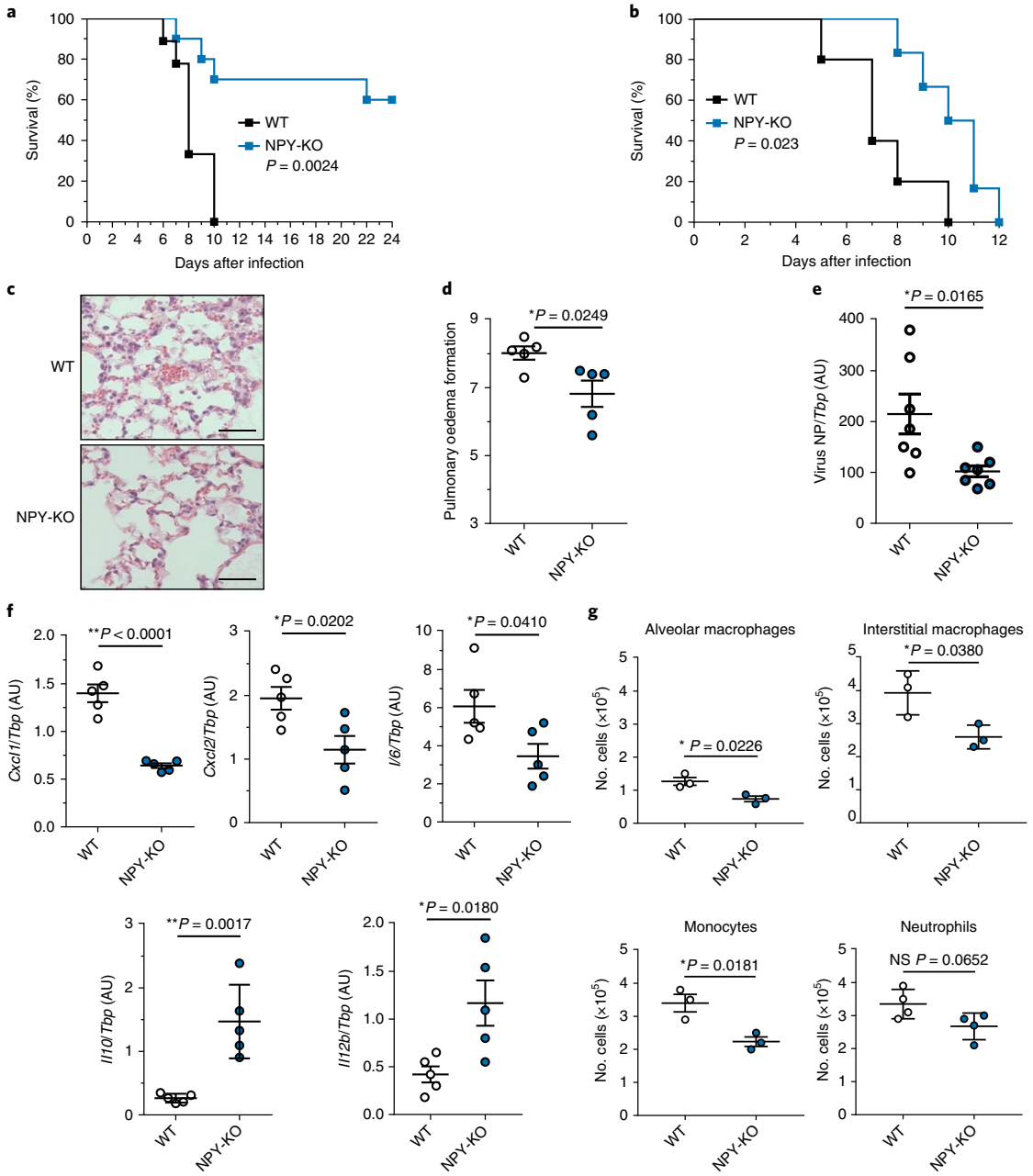

Fig. 2 | Deletion of NPY improves the pathology of severe influenza virus infection. a,**b**, Survival of wild-type (WT) and NPY-KO mice intratracheally infected with 56.2 $TCID_{50}$ PR8 virus (**a**; $n=10$ for WT and $n=10$ for NPY-KO) or 250 $TCID_{50}$ PR8 virus (**b**; $n=5$ for WT and $n=10$ for NPY-KO). Log-rank tests were performed. **c**–**f**, WT and NPY-KO mice were intratracheally infected with PR8 virus (56.2 $TCID_{50}$), and lung tissues were sampled 6 days after infection. Representative lung histopathology (H&E staining) image is shown (**c**; $n=4$ mice per group). Inflammatory cell infiltration, alveolar wall thickness and pulmonary haemorrhage were reduced in NPY-KO mice. Pulmonary oedema formation (**d**; $n=5$ mice per group; *y* axis shows wet/dry ratio), virus nucleoprotein (NP) mRNA expression (**e**; $n=7$ mice per group) and expression levels of cytokines (**f**; $n=5$ mice per group) in lung tissues are shown. Mean values were 214 and 102 in WT and NPY-KO, respectively (**e**). $^*P<0.05$ between the groups. $^{**}P<0.01$ between the groups. Unpaired two-tailed *t*-tests were used. **g**, WT and NPY-KO mice were infected with PR8 virus (100 $TCID_{50}$). Cells from the BAL fluids were obtained from the mice at day 5 and subjected to cell count and flow cytometry analyses. Cell numbers of alveolar macrophages, interstitial macrophages, monocytes and neutrophils are shown ($n=3$ mice per group). $^*P<0.05$ between the groups. Unpaired two-tailed *t*-tests were used. The data in **d**–**g** are presented as the mean ± s.e.m. Scale bars, 50 μm (**c**).

Chemical sympathectomy with 6-OHDA did not affect the changes in survival (Fig. 3i) and body weight loss (Supplementary Fig. 3c) in both $Y1R^{PC\text{-}WT}$ and $Y1R^{PC\text{-}KO}$ mice. In addition, virus replication (Fig. 3j) and pro-inflammatory cytokine mRNA expression (Fig. 3k) were comparable between vehicle- and 6-OHDA-treated $Y1R^{PC\text{-}WT}$ and $Y1R^{PC\text{-}KO}$ mice. These data again suggest that sympathetic neural NPY is unlikely to be involved in the Y1R-mediated pathology of severe influenza virus infection.

To further examine whether the NPY–Y1R axis acting on pulmonary phagocytes can control the pathology of severe influenza virus infection, we performed pulmonary macrophage depletion using clodronate before virus infection. In the clodronate-treated

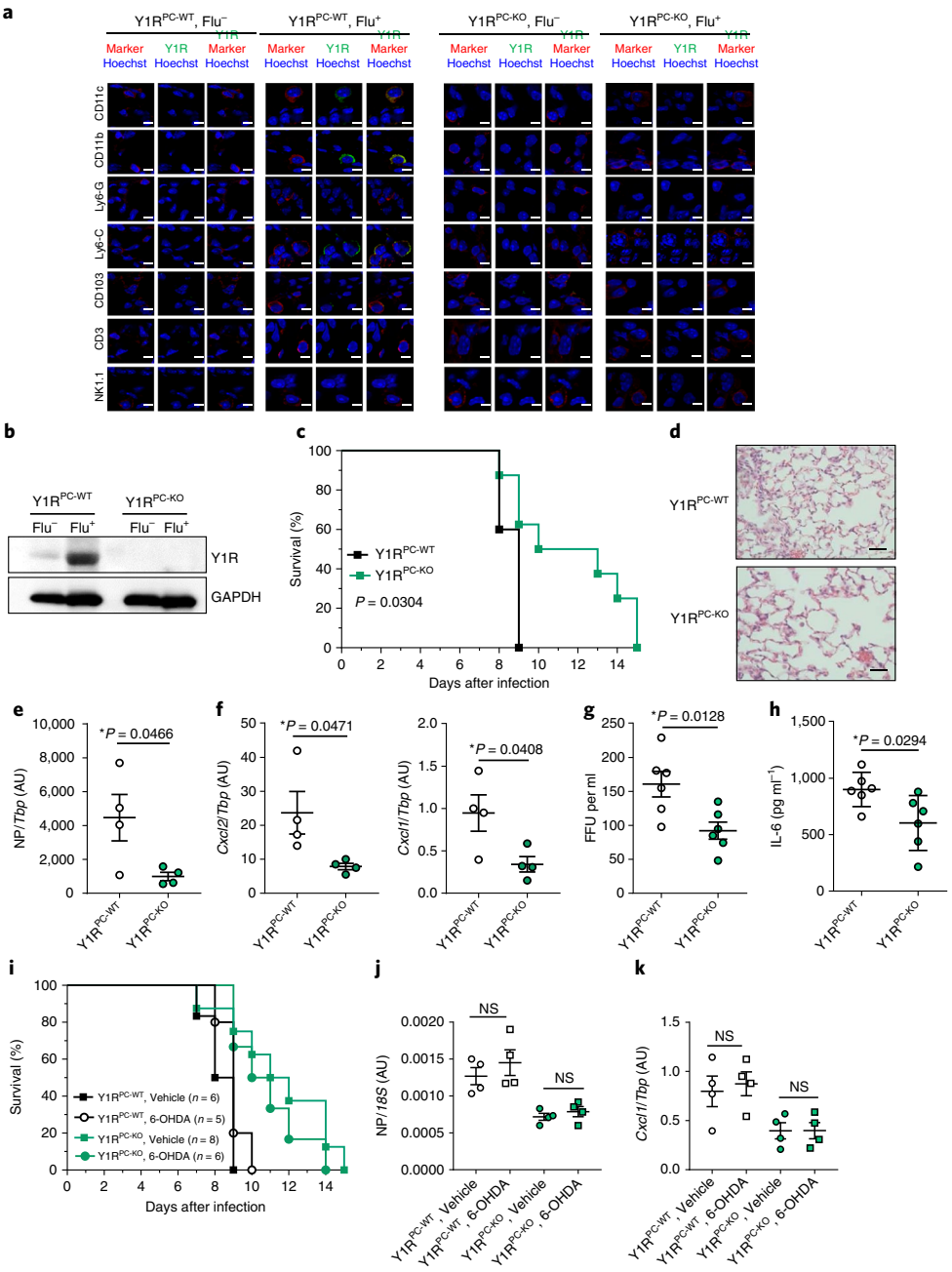

Fig. 3 | Phagocyte-specific NPY Y1R deletion improves the pathology of severe influenza virus infection. a, $Y1R^{PC\text{-}WT}$ and $Y1R^{PC\text{-}KO}$ mice were infected with mock or PR8 virus (100 $TCID_{50}$). Frozen lung sections were obtained from the animals at day 5 post infection and were co-stained with anti-Y1R antibody and antibodies against CD11c, CD11b, Ly6-G, Ly6-C, CD103, CD3 or NK1.1. Representative staining is shown ($n = 3$ mice per group). In the virus-infected wild-type lungs, Y1R was expressed on $CD11c^+$, $CD11b^+$ or Ly6-C^+ cells, but not Ly6-G^+, $CD103^+$, $CD3^+$ or $NK1.1^+$ cells. In $Y1R^{PC\text{-}KO}$ mice, Y1R was absent in all types of cells examined. **b**, Pulmonary myeloid cells were isolated from lung tissues of $Y1R^{PC\text{-}WT}$ and $Y1R^{PC\text{-}KO}$ mice at day 5 of the mock- or virus-infected conditions, and western blotting was performed using anti-Y1R antibody. Pulmonary myeloid cells obtained from $Y1R^{PC\text{-}KO}$ mice showed a loss of Y1R expression. Data are from three separate experiments. **c**, $Y1R^{PC\text{-}WT}$ mice ($n = 6$ per group) and $Y1R^{PC\text{-}KO}$ mice ($n = 8$ per group) were infected with PR8 virus (100 $TCID_{50}$). Survival of virus-infected $Y1R^{PC\text{-}WT}$ and $Y1R^{PC\text{-}KO}$ mice is shown. Log-rank tests were performed. **d**–**f**, $Y1R^{PC\text{-}WT}$ and $Y1R^{PC\text{-}KO}$ mice were infected with PR8 virus (100 $TCID_{50}$), and lung tissues were sampled 6 days after infection ($n = 4$ mice per group). Representative H&E staining images are shown (**d**). Inflammatory cell infiltration and alveolar wall thickness were reduced in $Y1R^{PC\text{-}KO}$ mice. Virus nucleoprotein (NP) mRNA (**e**), and *Cxcl1* and *Cxcl2* mRNA expressions (**f**) in lung tissues are shown. $^*P < 0.05$ between the groups. Unpaired two-tailed *t*-tests were used. **g**,**h**, Pulmonary phagocytes (macrophage and monocytes) were isolated from $Y1R^{PC\text{-}WT}$ and $Y1R^{PC\text{-}KO}$ mice, and the phagocytes were infected with PR8 virus (MOI of 5) for 18 h, and culture supernatant was collected. FFU (**g**) and IL-6 protein levels (**h**) in the supernatant are shown ($n = 6$ per group). $^*P < 0.05$ between the groups. Unpaired two-tailed *t*-tests were used. **i**–**k**, $Y1R^{PC\text{-}WT}$ and $Y1R^{PC\text{-}KO}$ mice were subjected to chemical sympathectomy with vehicle or 6-OHDA on day −7 (100 mg per kg), day −5 (100 mg per kg) and day −3 (200 mg per kg) and infected with PR8 virus (100 $TCID_{50}$) at day 0. Survival of the mice is shown (**i**). Log-rank tests were performed. In a separate experiment, lung tissues were sampled 6 days after infection. Nucleoprotein (NP) (**j**) and cytokine (*Cxcl1*) (**k**) mRNA expression levels in lung tissues are shown ($n = 4$ per group). One-way ANOVA was used. The data in **e**–**h** and **j**–**k** are presented as the mean ± s.e.m. Scale bars, 10 μm (**a**), 50 μm (**d**). For source images of the gels, see Supplementary Information.

lungs, cells expressing CD11b or CD11c disappeared 3 days after treatment, confirming the successful depletion of pulmonary phagocytes (Supplementary Fig. 4a). NPY expression was lower in the virus-infected lungs with macrophage depletion, further suggesting that NPY is mainly expressed in pulmonary phagocytes following virus infection (Supplementary Fig. 4b). After virus infection, body weight changes (Supplementary Fig. 4c), lung histology (Supplementary Fig. 4d) and virus nucleoprotein and cytokine expression (Supplementary Fig. 4e) were comparable between clodronate-treated $Y1R^{PC\text{-}WT}$ and $Y1R^{PC\text{-}KO}$ mice, suggesting that pulmonary macrophage depletion abolished the phenotype observed in $Y1R^{PC\text{-}KO}$ mice. Thus, our data further confirm that the NPY–Y1R axis on pulmonary phagocytes is critically involved in the pathology of severe influenza virus infection in vivo.

SOCS3 is controlled by NPY–Y1R signalling. Next, we examined the possible mechanisms by which the NPY–Y1R axis on pulmonary phagocytes can control the pathology of severe influenza virus infection. One candidate controlled by Y1R signalling is SOCS3[10–13], a protein suppressor of the JAK–STAT pathway. Consistent with a previous report[29], *Socs3* (Fig. 4a) but not *Socs1* (Fig. 4b) mRNA expression in lung tissues was increased in wild-type mice following virus infection; however, this was significantly lower in NPY-KO mice (Fig. 4a). In addition, the SOCS3 level was increased following virus infection in wild-type cells and in NPY-KO BAL cells, but the SOCS3 signal was weaker in the virus-infected NPY-KO cells compared with wild-type cells (Fig. 4c; Supplementary Fig. 4f). Furthermore, *Socs3* mRNA expression levels were not apparently different between control- and NPY-transfected mouse embryonic fibroblasts (MEFs) under non-infected conditions. In contrast, *Socs3* mRNA expression was increased following influenza virus infection as previously reported[29]. Importantly, higher virus titres yielded a greater induction of SOCS3 in the virus-infected cells, particularly under NPY-transfected conditions (Fig. 4d). Moreover, virus replication was enhanced in the wild-type cells transfected with NPY plasmid, while it was significantly suppressed in the SOCS3 knockout cells (Fig. 4e). NPY expression did not affect the virus replication in the SOCS3 knockout cells (Fig. 4e). Collectively, our data suggest that NPY expression controls SOCS3 induction during virus infection.

To test whether SOCS3 expression can control the pathology of severe influenza virus infection in vivo, we generated mice that had SOCS3 specifically knocked out in myeloid cells ($SOCS3^{MC\text{-}KO}$ mice) and subjected them to the severe influenza model. Compared with wild-type mice ($SOCS3^{MC\text{-}WT}$), $SOCS3^{MC\text{-}KO}$ mice had improved survival (Fig. 4f) and less virus replication (Fig. 4g) and pro-inflammatory cytokine expression (Fig. 4h) in virus-infected lung tissues. This result confirmed that SOCS3 activity is critically involved in virus replication and pro-inflammatory cytokine production in severe influenza virus infection in mice in vivo.

Similar to other viruses (that is hepatitis C virus[30], respiratory syncytial virus[31] and HIV[32]), it has been shown that SOCS3 inhibits STAT3-mediated interferon (IFN) signalling, resulting in enhanced virus replication in influenza virus infection[29]. Therefore, we examined whether the NPY–Y1R axis may be able to enhance virus replication through SOCS3-mediated inhibition of STAT3–IFN signalling. Compared with the wild type, SOCS3 levels in virus-infected pulmonary phagocytes were lower in NPY-KO mice and in $Y1R^{PC\text{-}KO}$ mice, coinciding with the enhanced phosphorylation of STAT3 (Fig. 4i). Furthermore, in the virus-infected lungs, IFN-α levels were higher in $Y1R^{PC\text{-}KO}$ (Fig. 4j, left panel) and $SOCS3^{MC\text{-}KO}$ mice (Fig. 4j, right panel) compared with wild-type mice, while IFN-α levels were comparable among the groups in the non-infected lungs. Thus, our data suggest that the NPY–Y1R axis is linked to SOCS3 expression, which may control STAT3-mediated IFN-α signalling, which in turn enhances virus replication.

NPY–Y1R–SOCS3 axis on phagocytes enhances pulmonary inflammation in parallel to virus replication in influenza virus infection. Next, to examine the role of the NPY–Y1R axis in global gene expression, we performed a RNA-seq analysis of pulmonary phagocytes isolated from non-infected and infected wild-type mice ($Y1R^{PC\text{-}WT}$) and $Y1R^{PC\text{-}KO}$ mice. The binding motifs of MYC and ETV family of proteins, and stress-responsive transcription factors (that is, USP1), which are known to control cellular damage and inflammation[33], were over-represented only in the promoter sequences of upregulated genes in the wild-type mice (Fig. 5a, magenta circles), while those of STAT1, STAT3 and STAT4 were highly enriched only in $Y1R^{PC\text{-}KO}$ mice (Fig. 5a, light blue circles). These results suggest that activation of the NPY–Y1R axis is linked to enhanced cellular damage and inflammatory responses and reduced STAT-mediated IFN responses.

However, it remains unknown whether activation of the NPY–Y1R–SOCS3 axis can suppress antiviral IFN responses, thereby leading to increased virus replication and consequently enhanced inflammation, or whether the enhanced inflammation is induced in parallel to reduce antiviral IFN responses. To test this, mice were intratracheally injected with replication-defective dsRNA (polyinosinic:polycytidylic acid (Poly I:C)). First, intratracheal Poly I:C treatment induced the expression of NPY, SOCS3, pro-inflammatory cytokines and IFN-α (Supplementary Fig. 5a,b,c) in lungs of wild-type mice. This result suggests that intratracheal Poly I:C treatment mimics the viral pulmonary inflammation process[34]. Next, $Y1R^{PC\text{-}WT}$ and $Y1R^{PC\text{-}KO}$ mice were treated with intratracheal Poly I:C. The lung histology was slightly improved in $Y1R^{PC\text{-}KO}$ mice after Poly I:C treatment (Fig. 5b). In addition, the expression of NPY (Fig. 5c) and pro-inflammatory cytokines (Fig. 5d) in lung tissues was decreased in $Y1R^{PC\text{-}KO}$ mice. Similar to live virus infection (Fig. 4i), SOCS3 expression was reduced in lungs of $Y1R^{PC\text{-}KO}$ mice, whereas STAT3 phosphorylation was comparable between the groups (Fig. 5f), suggesting a potential STAT-independent regulation of inflammation by SOCS3[12].

Collectively, our data indicate that influenza virus infection induces the expression of NPY and its Y1R in pulmonary phagocytes. Activation of the NPY–Y1R axis on phagocytes triggers SOCS3 induction, which enhances virus replication through the suppression of phosphorylated STAT3-mediated IFN responses. In parallel, this leads to the enhancement of pulmonary inflammation, thereby contributing to the pathogenesis of severe influenza virus infection. Thus, the NPY–Y1R–SOCS3 axis on phagocytes could be a novel therapeutic target for severe influenza virus infection.

Discussion

In the present study, we demonstrated that NPY promoter activity and synthesis, as well as Y1R expression, are upregulated in pulmonary phagocytes following influenza virus infection. Presumably, the activation of transcription factors including immediate-early genes (that is, *Jun*, *JunB* and *Egr1*) is involved in *Npy* expression following influenza virus infection. This finding is consistent with reports that Foxp1- and Foxp4-mediated NPY generation by epithelial cells can induce smooth muscle construction[35]. Many external stimuli, including cytokines, growth factors, Toll-like receptor ligands, components of the Hippo pathway (that is, Yap) and hormones (that is, leptin), can induce SOCS3 expression[10–13], which can modulate the response to the stimuli in a STAT3-dependent or -independent manner[12]. We found that influenza virus infection induces the activation of the NPY–Y1R axis on phagocytes, which triggers SOCS3 induction, leading to virus replication through the suppression of STAT3-mediated IFN responses. In parallel, STAT3-independent pulmonary inflammation is enhanced, thereby aggravating the pathology of severe influenza virus infection.

In addition to respiratory epithelial cells, influenza virus, in particular the highly pathogenic H5N1 virus, can infect macrophages

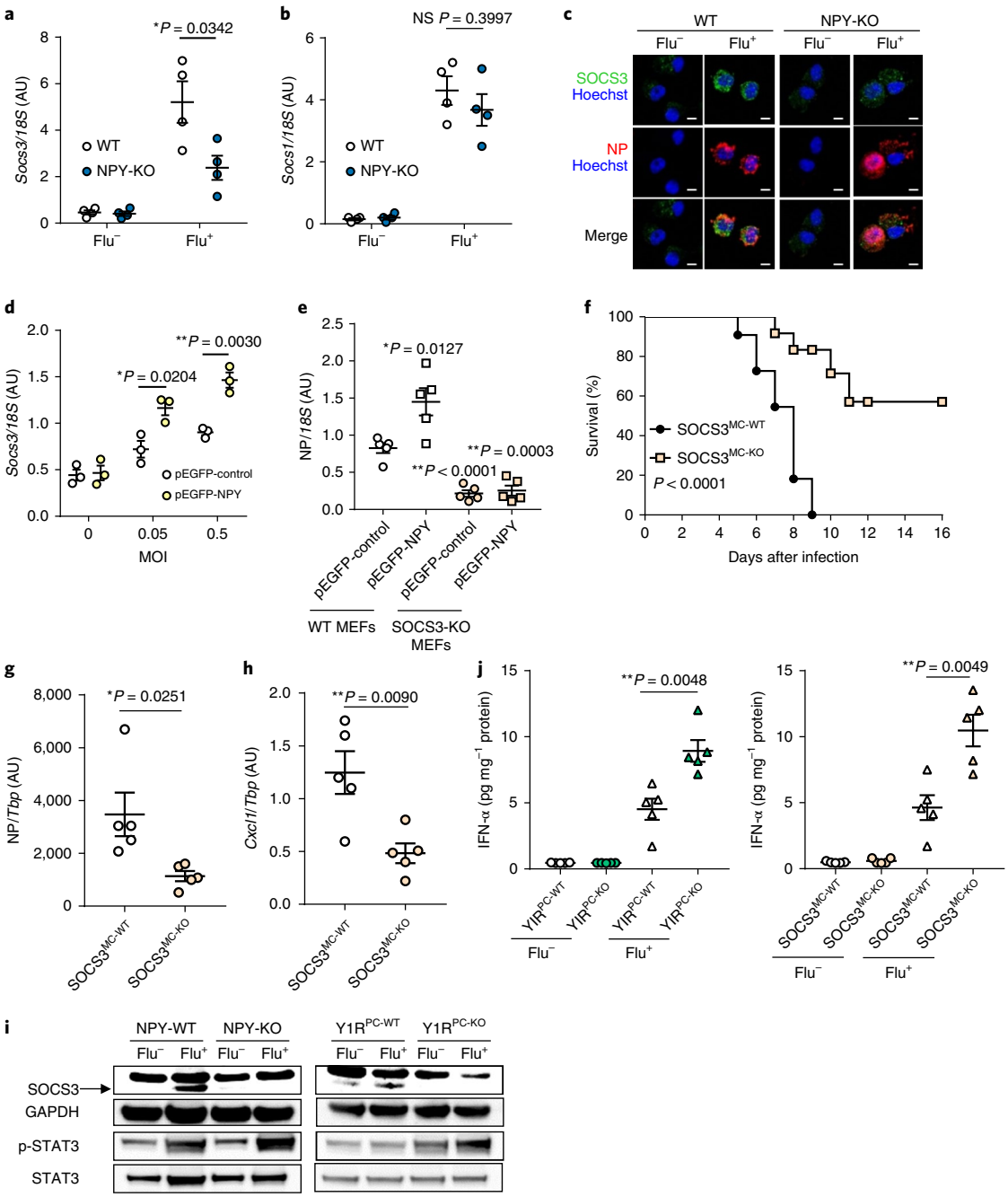

Fig. 4 | SOCS3 is involved in the NPY–Y1-mediated pathology of severe influenza virus infection. a,**b**, Wild-type (WT) and NPY-KO mice were infected with mock or PR8 virus (100 $TCID_{50}$), and lung tissues were sampled at day 6. mRNA expression of *Socs3* (**a**) and *Socs1* (**b**) in lung tissues are shown ($n = 4$ per group). $^{*}P < 0.05$ between the groups. One-way ANOVA was used, and if significant, further analysed by two-tailed *t*-tests. **c**, BAL fluid was collected from mock- or virus-infected WT and NPY-KO mice at 2 days after infection. Cells in BAL fluid were stained using nucleoprotein (NP)-specific and SOCS3-specific antibodies. Representative images are shown ($n = 3$ per group). **d**, WT MEFs were transfected with control or NPY plasmid and infected with different MOIs (0, 0.05 or 0.5) of PR8 virus for 8 h. *Socs3* mRNA expression of the cells is shown. $^{*}P < 0.05$ and $^{**}P < 0.01$ between the groups. Unpaired two-tailed *t*-tests were used. Data are from three separate experiments. **e**, MEFs obtained from WT and SOCS3-KO were transfected with control or NPY plasmid and infected with mock or PR8 virus (MOI of 0.5) for 8 h. Virus NP mRNA expression of the cells is shown. $^{*}P < 0.05$ and $^{**}P < 0.01$ compared to control-transfected wild-type cells. One-way ANOVA was used, and if significant, further analysed by two-tailed *t*-tests. Data are from five separate experiments. **f**, $SOCS3^{MC\text{-}WT}$ ($n = 10$) and $SOCS3^{MC\text{-}KO}$ ($n = 11$) mice were infected with PR8 virus (50 $TCID_{50}$). Survival of virus-infected $SOCS3^{MC\text{-}WT}$ and $SOCS3^{MC\text{-}KO}$ mice are shown. Log-rank tests were performed. **g**,**h**, $SOCS3^{MC\text{-}WT}$ and $SOCS3^{MC\text{-}KO}$ mice were infected with PR8 virus (50 $TCID_{50}$), and lung tissues were sampled 2 days after infection. NP (**g**) and *Cxcl1* (**h**) mRNA expression in lung tissues are shown ($n = 5$ per group). $^{*}P < 0.05$ and $^{**}P < 0.01$ between the groups. Unpaired two-tailed *t*-tests were used. **i**, WT and NPY-KO mice, as well as $Y1R^{PC\text{-}WT}$ and $Y1R^{PC\text{-}KO}$ mice, were infected with mock or PR8 virus (100 $TCID_{50}$), and lung myeloid cells were isolated at day 2. Western blots of SOCS3, GAPDH, phosphorylated STAT3 (p-STAT3) and STAT3 are shown. Data are from three separate experiments. **j**, $Y1R^{PC\text{-}WT}$, $Y1R^{PC\text{-}KO}$, $SOCS3^{MC\text{-}WT}$ and $SOCS3^{MC\text{-}KO}$ mice were infected with mock or PR8 virus (100 $TCID_{50}$), and lung tissues were sampled at day 2. IFN-α levels of the lung tissues are shown ($n = 5$ mice per group). $^{**}P < 0.01$ between the groups. One-way ANOVA was used, and if significant, further analysed by two-tailed *t*-tests. The data in **a**, **b**, **d**, **e**, **g**, **h** and **j** are presented as the mean ± s.e.m. Scale bars, 10 μm (**c**). For source images of the gels, see Supplementary Information.

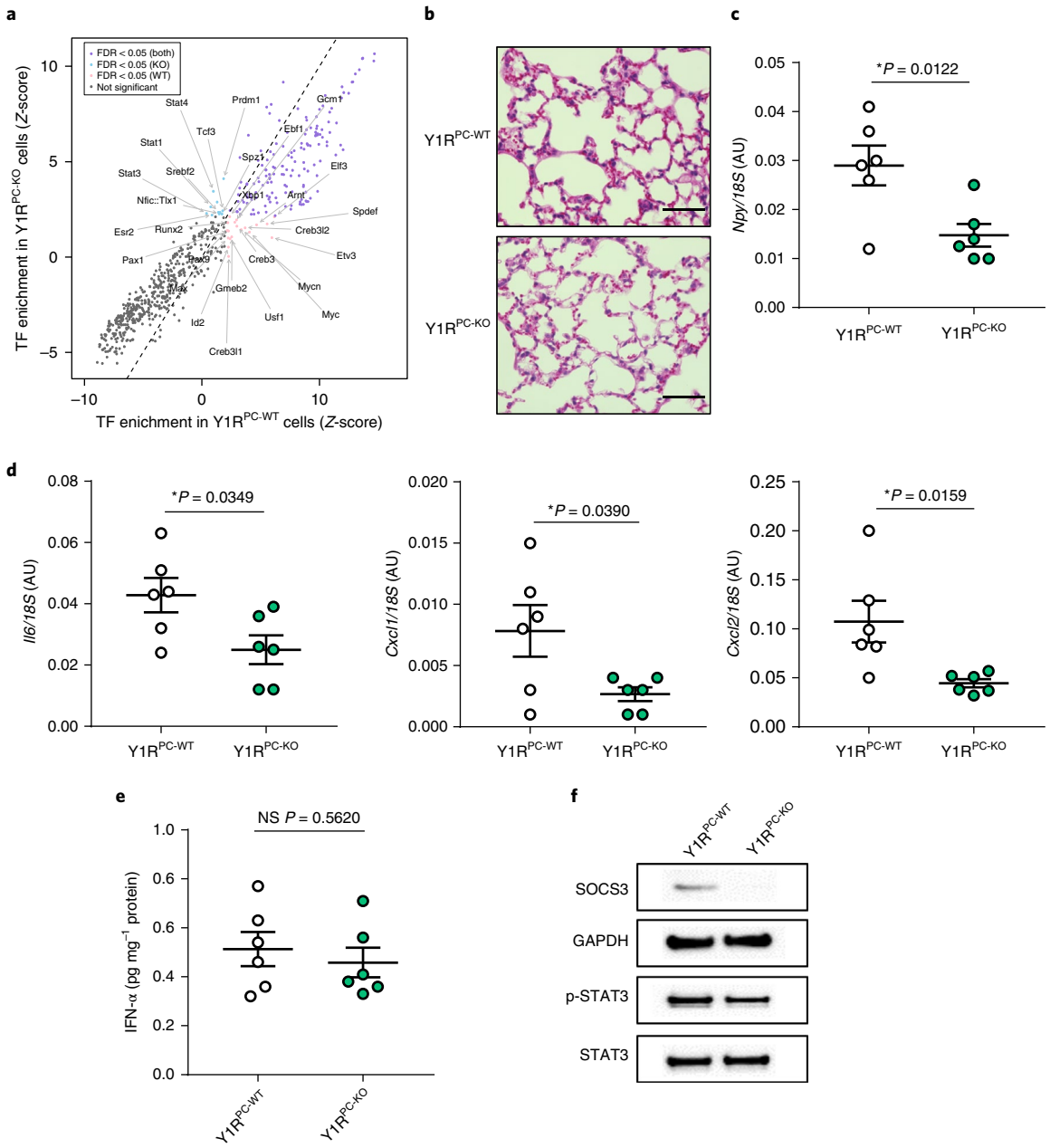

Fig. 5 | The NPY–Y1R–SOCS3 axis on phagocytes enhances pulmonary inflammation in parallel to virus replication in influenza virus infection. a, $Y1R^{PC\text{-}WT}$ and $Y1R^{PC\text{-}KO}$ mice were mock- or virus-infected for 24 h and RNA-seq of the pulmonary phagocytes isolated from the mice was performed ($n = 3$ mice per group). A scatter plot of over-represented transcription factor (TF)-binding motifs in co-upregulated genes in $Y1R^{PC\text{-}WT}$ and $Y1R^{PC\text{-}KO}$ phagocytes after virus infection is shown. The axes indicate the *Z*-score of transcription factor-binding motif enrichment in the promoter sequences of upregulated genes compared to genome-wide promoters. Purple, magenta and light blue circles indicate genes that were significantly (FDR < 0.05) different in both conditions, in $Y1R^{PC\text{-}WT}$ cells only, and $Y1R^{PC\text{-}KO}$ cells only, respectively. Names of representative transcription factor-binding motifs shown in blue and magenta circles are indicated. **b**–**e**, $Y1R^{PC\text{-}WT}$ ($n = 6$) and $Y1R^{PC\text{-}KO}$ ($n = 6$) mice were intratracheally treated with Poly I:C (50 μg per mouse) and lungs were collected 2 days after treatment. A representative lung histology (H&E staining) image is shown (**b**). Inflammatory cell infiltration and pulmonary oedema formation were slightly reduced in the lungs of Poly I:C-treated $Y1R^{PC\text{-}KO}$ mice. mRNA expression levels of *Npy* (**c**) and cytokines (**d**) in lung tissues are shown. IFN-α levels of the lung tissues are shown (**e**). $^*P < 0.05$ between the groups. Unpaired two-tailed *t*-tests were used. **f**, $Y1R^{PC\text{-}WT}$ and $Y1R^{PC\text{-}KO}$ mice were intratracheally treated with Poly I:C (50 μg per mouse) and lung tissues were isolated at day 2. Western blots of SOCS3, GAPDH, p-STAT3 and STAT3 are shown. Data are from three separate experiments. The data in **c**–**e** are presented as the mean ± s.e.m. Scale bars, 50 μm (**b**). For source images of the gels, see Supplementary Information.

and monocytes, although a consensus on its general impact on the pathogenesis of influenza virus infection has not been reached[24]. In the present study, we showed that lack of NPY in mice can ameliorate the disease pathology following not only PR8 virus but also pandemic H1N1/2009 virus infection, both of which are known to infect macrophages and monocytes[24,25]. Thus, the virus strains that have the capacity to replicate productively in macrophages and monocytes may control the pathogenesis of severe influenza through an NPY–Y1R–SOCS3 pathway on phagocytes.

Similar to catecholamines[9,10], NPY is an important component of the 'fight or flight' response to threatening situations (that is, pathogens, diet or stress). Recent studies have shown that stress is associated with elevated peripheral NPY levels, which was observed to be associated with exacerbated airway inflammation in asthma[35,36]. In addition, NPY has been shown to be produced by adipose tissue macrophages from obese individuals, and takes part in the regulation of obesity-induced inflammation[37]. Our data suggest that the NPY–Y1R axis might be involved in the pathogenesis of severe influenza virus infection in patients, in particular those with high risk factors such as asthma and obesity. Thus, in addition to the sympathetic neural regulation of NPY, our data suggest that self-regulatory mechanisms on phagocytes mediated via the NPY–Y1R–SOCS3 pathway could act as fine-tuners of the innate immune response to influenza virus infection, and this axis might be a unique therapeutic target for severe influenza virus infection.

Methods

No statistical methods were used to predetermine sample sizes. The experiments were not randomized and the investigators were not blinded to allocation during experiments and outcome assessments.

Mice. NPY-KO, NPY-GFP and M lysozyme-Cre[28] mice were obtained from Jackson Laboratory. The background of NPY-KO mice was 129/SvJ. 129/SvJ mice were bred at our animal facility. Y1R-floxed[27] and SOCS3-floxed mice[38] were generated as previously described. Y1R-floxed and SOCS3-floxed mice were crossed with the M lysozyme-Cre recombinase strain to generate myeloid cell-specific Y1R and SOCS3 knockout mice, respectively. For all in vivo experiments, male mice aged between 8 and 12 weeks were used. Mice were allocated to experimental groups on the basis of genotype- and age-matching. All animal procedures were performed according to the protocols provided by the Institutional Animal Care and Use Committee of Akita University and the National Institutes of Biomedical Innovation, Health and Nutrition.

Viruses. H1N1/PR8 and H1N1/2009 influenza virus strains were used. All infection experiments were performed under biosafety level 2 conditions.

Intratracheal influenza virus infection in mice. Intratracheal influenza virus infection of mice was conducted as previously described[16,17]. In brief, mice were anaesthetized via an intraperitoneal injection of ketamin (75 mg per kg) and xylazine (20 mg per kg). A 24-gauge intravenous catheter was inserted into the trachea, and mice received either a suspension of influenza virus in 50 µl of PBS. Mice were monitored and weighed daily post infection.

Alveolar macrophage depletion in mice. Alveolar macrophage depletion was performed as previously described[39]. In brief, mice were anaesthetized via an intraperitoneal injection of medetomidine hydrochloride (0.3 mg per kg), midazolam (1.6 mg per kg) and butorphanol tartrate (2 mg per kg). A 24-gauge intravenous catheter was inserted into the trachea, and mice received either 100 µl of control or clophosome-A (referred to as clodronate) (Funakoshi). Three days after injection of clodronate or control, anaesthetized mice were intratracheally infected with influenza virus as described above. Mice were monitored and weighed daily post infection. Lung tissues were sampled at indicated time points.

Poly I:C treatment in mice. Mice were anaesthetized via an intraperitoneal injection of medetomidine hydrochloride (0.3 mg per kg), midazolam (1.6 mg per kg) and butorphanol tartrate (2 mg per kg). A 24-gauge intravenous catheter was inserted into the trachea. Poly I:C treatment was performed as previously described[34]. In brief, mice received vehicle or 50 µg of Poly I:C HMW (Invivogen) intratracheally, and lung tissues were samples 2 days after treatment.

Chemical sympathectomy in mice. For sympathectomy with 6-OHDA, mice were injected intraperitoneally with 6-OHDA (Sigma-Aldrich) or vehicle in 0.9% NaCl plus 10^{-7} M ascorbic acid on day −7 (100 mg per kg), day −5 (100 mg per kg) and day −3 (200 mg per kg), as previously described[40]. For sympathectomy with reserpine, mice were injected intraperitoneally with reserpine (TOCRIS Bioscience) (5 mg kg) or vehicle on day −5, as previously described[5].

$TCID_{50}$ and focus forming unit assays. 50% tissue culture infective dose ($TCID_{50}$) and focus forming unit (FFU) assays were performed as previously described[16,17,41]. In brief, for $TCID_{50}$ assays, aliquots of culture supernatants or tissue lysates were serially diluted, applied to 2×10^4 MDCK cells per well of a 96-well plate, and incubated at 37 °C for 1 h. The inoculum was removed, and the cells were washed with PBS and supplied with DMEM containing 0.2% bovine serum albumin and trypsin (5 µg ml^{-1}). On the third day after infection, the $TCID_{50}$ was determined on the basis of the Karber method. For the FFU assay, MDCK cells were plated at 2×10^4 MDCK cells per well of a 96-well plate. At 24 h after infection with serially diluted supernatants or tissue lysates containing virus, the cells were fixed with paraformaldehyde in PBS containing 0.1% Triton X-100 and washed with PBS three times. Antibody that reacts with common sequences of the influenza virus nucleoprotein (NP). Antibody binding to viral proteins was detected with an Alexa Fluor 488-conjugated secondary antibody (A21206, Invitrogen).

Pulmonary oedema formation. Pulmonary oedema was assessed by measuring the lung wet/dry weight ratio as previously described[42,43]. In brief, the lobe of the lung was rinsed and weighed to obtain the wet weight and then placed in an oven at 75 °C for 48 h for subsequent measurement of the dry weight. The wet/dry weight ratio was then calculated.

Histopathology and lung injury score. The lung lobes were fixed in buffered 10% formalin and then embedded in paraffin. Sections were cut into 5-µm slices and stained with haematoxylin and eosin (H&E) for light microscopy. The histopathology was reviewed in a blinded manner using a modified histological scoring system as previously described[17,44]. Pathologies were graded on a scale of 0–4 based on alveolar congestion, haemorrhage, leukocyte infiltration or aggregation of neutrophils in the airspace or the vessel wall, and thickness of the alveolar wall. Histopathological changes were scored as follows: 0 represented normal lungs; 1 represented mild change; 2 moderate changes; 3 severe changes; and 4 very severe changes. The results of the histopathological changes are expressed as the mean ± s.e.m. For immunohistochemistry analyses of paraffin sections of lung tissue obtained from NPY-GFP mice, GFP-specific antibody (M048-3, MBL) and tyrosine hydroxylase (AB152, Millipore) were used for NPY-GFP and tyrosine hydroxylase staining, respectively.

Immunohistochemistry and immunofluorescence. For the immunohistochemistry analyses of frozen lung sections, lungs collected from mice were immediately frozen in liquid nitrogen, and the sections were cut into 5-µm slices and incubated with Y1R-specific antibody (sc-28949, SantaCruz), and then incubated with Alexa 488 antibody (A21206, Invitrogen) and CD11c-PE (557401, BD), CD11b-PE (12-0112-81, eBioscience), Ly6-C-PE (128007, BioLegend), Ly6-G-PE (127607, BioLegend), Siglec-F-PE (552126, BD), CD103-PE (2-1031-82, eBioscience), NK1.1-PE (108707, BioLegend) or CD3-PE (12-0041-81, eBioscience). Cover slips were mounted on the slides with mounting medium (Dako) containing Hoechst (ThermoFisher). Images were visualized using a Leica Microsystems, TCS SP8, LASX DMI6000. For immunofluorescence, BAL (1 ml of PBS, 3 times) was performed in wild-type or NPY-GFP mice. BAL smears were subjected to immunofluorescence. For staining of NPY-GFP and leukocytes expressing specific markers, the cells were incubated with an NPY-GFP-specific antibody (ab5450, Abcam) and then incubated with appropriate combinations of Alexa 488 antibody (A21206, A11055, A31570; Invitrogen) and antibodies for CD11c-PE (557401, BD), CD11b-PE (12-0112-81, eBioscience), Ly6-C-PE (128007, BioLegend), Ly6-G-PE (127607, BioLegend), Siglec-F-PE (552126, BD), CD103-PE (2-1031-82, eBioscience), NK1.1-PE (108707, BioLegend) or CD3-PE (12-0041-81, eBioscience). For Y1R or Y2R and CD11c or CD11b double-staining, BAL smears were incubated with an anti-GFP antibody (ab5450, Abcam), anti-Y1R antibody (sc-28949, SantaCruz) or anti-Y2R antibody (RA14112, Neuromics), and then incubated with appropriate combinations of Alexa 488 antibody and CD11c-PE or CD11b-PE antibody. For SOCS3 staining, BAL smears were stained using an anti-SOCS3 antibody (18395, IBL). Cover slips were mounted on slides with mounting medium (Dako) containing Hoechst (ThermoFisher). Images were visualized using an A1Rsi confocal microscope (Nikon). For quantification of the images, different fields were selected at ×40 magnification, and a percentage score was calculated by dividing the number of the indicated cells by the total number of cells counted.

Flow cytometry analysis of BAL cells. BAL was performed in non-infected and infected NPY-GFP, wild-type or NPY-KO mice as described above, and the BAL fluids were passed through 40-µm nylon mesh to obtain a single-cell suspension. The cell number in BAL fluids was counted using an Auto-cell counter (R1-SET, Olympus) or a Neubauer haemacytometer (Fisher). Dead cells were identified by using trypan blue and then excluded. Flow cytometry analyses were performed as previously described[19–21]. In brief, cells were incubated with a Fc receptor block (BD Biosciences), and stained using the reagents listed in Supplementary Table 1. Viability was assessed by staining using a Zombie NIR Fixable Viability kit (BioLegend) or propidium iodide (BD Biosciences). Data were acquired on an Accuri C6F flow cytometer (BD Biosciences), and data analyses were performed using Accuri C6 software (BD Biosciences). For the analyses of cell types in BAL fluids of NPY-GFP (Fig. 1e; Supplementary Fig. 1c), wild-type and NPY-KO mice (Fig. 2g; Supplementary Fig. 2c), the following markers were used: alveolar macrophages were identified as $CD11c^+$ and Siglec-F^+; interstitial macrophages as $CD11b^+$ and $F4/80^+$; monocytes as $CD11b^+$ and Ly6-C^+; neutrophils as $CD11b^+$ and Ly6-G^+; mDCs as $CD11c^+$ and $CD103^+$; $CD3^+$ T cells as $CD3^+$; and NK cells as $NK1.1^+$. For the analyses of NPY-GFP expression of the individual cells types in BAL fluids of NPY-GFP mice (Fig. 1e; Supplementary Fig. 1c), data from wild-type mice served as controls.

Isolation and virus infection of lung macrophages. Lung macrophages were prepared as previously described[42]. In brief, lung tissues were excised from mice and finely minced, and the tissue pieces placed in RPMI medium containing 20 U ml^{-1} collagenase Type I (Sigma-Aldrich) and 1 μg ml^{-1} DNase. Following incubation, any remaining intact tissue was disrupted by passage through a 40-μm cell strainer. The digested cell suspension was then layered on 50% Ficoll (GE Healthcare), centrifuged at 400 *g* for 40 min and the macrophage layers were collected. The cells were cultured with RPMI medium containing 10% fetal calf serum (FCS), 20 U ml^{-1} penicillin, 20 μg ml^{-1} streptomycin and 2 mM L-glutamine in an incubator at 37 °C with 5% CO_2. For virus infection, isolated macrophages were plated on 96-well plates and then infected with influenza virus (PR8 strain) at the indicated multiplicity of infection (MOI) values in RPMI without FCS for 60 min at 37 °C. Cells were washed and incubated for the indicated time periods at 37 °C in RPMI supplemented with 10% FCS. Aliquots of the supernatants were collected and subjected to FFU or ELISA assays.

MEFs. MEFs were obtained from embryonic day 13.5 *Socs3*$^{fl/fl}$ embryos as previously described[45]. To delete the *Socs3* gene, MEFs were infected with an adenovirus carrying Cre-recombinase at 500 MOI and cultured. We did not observe any *Socs3* expression for at least 6 months.

Virus infection of MEFs. Virus infection of MEFs was performed as previously described[16,17]. In brief, MEFs were grown in DMEM (Sigma) supplemented with 10% FCS (Equitechbio) at 37 °C and 5% CO_2. For influenza virus infection, cells on culture plates were washed twice with PBS and then infected with virus at the indicated MOI values in DMEM without FCS for 60 min at 37 °C. Cells were washed and incubated for the indicated time periods at 37 °C in DMEM supplemented with 10% FCS. Cell lysates prepared from infected cells after the removal of media were used for real-time quantitative PCR as described below.

Plasmid transfection. The coding sequence of mouse *Npy* was cloned into pEGFPN3 (Addgene) using an In-Fusion HD Cloning kit (Takara). pEGFPN3-NPY or mock plasmids (pEGFPN3-control) were transfected into MEFs using Nucleofector (Lonza). Forty-eight hours after transfection, cells were used for further experiments.

Western blotting. Proteins of mouse lungs or phagocytes were extracted with TNE lysis buffer (50 mM Tris, 150 mM NaCl, 1 mM EDTA, 1% NP40, protease inhibitor (complete Mini, Roche), 100 mM NaF, 2 mM Na_3VO_4) as previously described[17]. After sonication and denaturation with LDS sample buffer (Invitrogen) at 70 °C, proteins were electrophoresed on NuPAGE Bis-Tris precast gels (Invitrogen) and transferred to nitrocellulose membranes (0.2 mm pore, Invitrogen). Membranes were probed with the following antibodies; anti-SOCS3 (18395, IBL); phospho-STAT3 (Tyr705) (9145, CST); STAT3 (12640, CST); Y1R (sc-28949, SantaCruz); or GAPDH (2118, CST). Specific bands were visualized by secondary antibody conjugated to horseradish peroxidase and ECL Western Blotting Detection Reagents (GE Healthcare) using Image Quant LAS4000 (GE Healthcare).

Real-time quantitative PCR. The expression levels of PR8 virus nucleoprotein mRNA and host mRNAs were measured by real-time PCR as previously described[16,17]. Briefly, RNA was extracted from cells using a RNeasy Mini kit (Qiagen). First-strand complementary DNA was synthesized from DNA-free RNA using a Primescript RT reagent kit (Takara). Samples of first-strand cDNA were subjected to real-time PCR quantification (Thermal Cycler Dice Real Time System II, Takara) using specific primers for the indicated RNAs with *Tbp* or *18S* as an internal control. Relative amounts of RNA were calculated using the comparative CT method.

ELISA. Frozen lung tissues were homogenized in cell lysis buffer, and supernatants were assayed using specific ELISA kits to detect murine NPY (Phoenix Pharmaceuticals), IL-6 (R&D Systems) and IFN-α (R&D Systems).

RNA-seq library preparation, sequencing and analysis. Library preparation was performed using a TruSeq stranded mRNA Sampleprep kit (Illumina) according to the manufacturer's instructions. Sequencing was performed on an Illumina HiSeq 2500 platform in a 75-base single-end mode. Illumina Casava software was used for base calling. For data processing, sequence reads were trimmed by using Trim Galore! (Babraham Institute, https://www.bioinformatics.babraham.ac.uk/projects/trim_galore/), and then mapped to a reference mouse genome (mm10) using HISAT2[46] with the default settings. Gene expression profiles were quantified from the aligned data using featureCounts[47]. To identify the differentially expressed genes, read counts in each condition in triplicate were analysed using edgeR[48], and the false discovery rate (FDR) was calculated. Genes whose expression levels were increased by influenza virus infection in Y1R$^{PC\text{-}WT}$ and Y1R$^{PC\text{-}KO}$ mice were determined using the following criteria: FDR < 0.05 and log2 fold change of >0.5.

Transcription factor-binding motif analysis. Transcription factor-binding motifs at the promoter region of *Npy* (from 450 bp upstream of the TSS to 50 bp downstream of the TSS) were searched using the CIS-BP database (http://cisbp.ccbr.utoronto.ca)[22] with the following parameters: Motif model, PWMs – Energy; Threshold, 0.2. Transcription factor-binding motifs over-represented in the promoter region of upregulated genes in Y1R$^{PC\text{-}WT}$ and Y1R$^{PC\text{-}KO}$ mice were analysed using Pscan (http://www.beaconlab.it/pscan)[49] with the following settings: Region, −450 + 50; Descriptors, Jasper 2016.

Statistical analyses. Statistical significance was determined using GraphPad Prism 5 or 6. Measurements at single time points were analysed using unpaired *t*-tests or analysis of variance (ANOVA) according to test requirements. Time courses were analysed by repeated measurements (mixed model) of ANOVA. Variance was similar between groups. Log-rank tests were performed on Kaplan–Meier survival curves. No inclusion or exclusion criteria were pre-established. Grubbs' Outlier Test was used to determine outliers, which were excluded from the final analysis. *P* values of <0.05 (indicated by one asterisk), <0.01 (indicated by two asterisks) or <0.001 were considered significant. The FDR was adjusted using the Benjamini–Hochberg method.

The antibodies used in this study are listed in Supplementary Table 1.

The sequences for quantitative PCR primers used in this study are listed in Supplementary Table 2.

Reporting Summary. Further information on research design is available in the Nature Research Reporting Summary linked to this article.

Data availability

Nucleotide sequencing data that support the findings of this study have been deposited in Sequenced Read Archive in the DNA Data Bank of Japan (DDBJ) and are available under the accession number DRA007253. The data that support the findings of this study are available from the corresponding author upon request.

Received: 18 January 2018; Accepted: 10 October 2018;
Published online: 19 November 2018

References

1. Clark, N. M. & Lynch, J. P. 3rd. Influenza: epidemiology, clinical features, therapy, and prevention. *Semin. Respir. Crit. Care Med.* **32**, 373–392 (2011).
2. Beigel, J. H. et al. Avian influenza A (H5N1) infection in humans. *N. Engl. J. Med.* **353**, 1374–1385 (2005).
3. Tracey, K. J. The inflammatory reflex. *Nature* **420**, 853–859 (2002).
4. Sternberg, E. M. Neural regulation of innate immunity: a coordinated nonspecific host response to pathogens. *Nat. Rev. Immunol.* **6**, 318–328 (2006).
5. Flierl, M. A. et al. Phagocyte-derived catecholamines enhance acute inflammatory injury. *Nature* **449**, 721–725 (2007).
6. Lundberg, J. M., Rudehill, A., Sollevi, A., Fried, G. & Wallin, G. Co-release of neuropeptide Y and noradrenaline from pig spleen in vivo: importance of subcellular storage, nerve impulse frequency and pattern, feedback regulation and resupply by axonal transport. *Neuroscience* **28**, 475–486 (1989).
7. Bedoui, S. et al. Relevance of neuropeptide Y for the neuroimmune crosstalk. *J. Neuroimmunol.* **134**, 1–11 (2003).
8. Wheway, J., Herzog, H. & Mackay, F. NPY and receptors in immune and inflammatory diseases. *Curr. Top. Med. Chem.* **7**, 1743–1752 (2007).
9. Dimitrijevic, M. & Stanojevic, S. The intriguing mission of neuropeptide Y in the immune system. *Amino Acids* **45**, 41–53 (2013).
10. Yoshimura, A., Naka, T. & Kubo, M. SOCS proteins, cytokine signalling and immune regulation. *Nat. Rev. Immunol.* **7**, 454–465 (2007).
11. Linossi, E. M., Babon, J. J., Hilton, D. J. & Nicholson, S. E. Suppression of cytokine signaling: the SOCS perspective. *Cytokine Growth Factor Rev.* **24**, 241–248 (2013).
12. Carow, B. & Rottenberg, M. E. SOCS3, a major regulator of infection and inflammation. *Front. Immunol.* **5**, 58 (2014).
13. Mahony, R., Ahmed, S., Diskin, C. & Stevenson, N. J. SOCS3 revisited: a broad regulator of disease, now ready for therapeutic use? *Cell. Mol. Life Sci.* **73**, 3323–3336 (2016).
14. Vijayakumar, P. et al. Analysis of the crow lung transcriptome in response to infection with highly pathogenic H5N1 avian influenza virus. *Gene* **559**, 77–85 (2015).
15. Ahmed, C. M., Dabelic, R., Bedoya, S. K., Larkin, J. 3rd & Johnson, H. M. A SOCS1/3 antagonist peptide protects mice against lethal infection with influenza a virus. *Front. Immunol.* **6**, 574 (2015).
16. Ichikawa, A. et al. CXCL10–CXCR3 enhances the development of neutrophil-mediated fulminant lung injury of viral and nonviral origin. *Am. J. Respir. Crit. Care Med.* **187**, 65–77 (2013).
17. Morita, M. et al. The lipid mediator protectin D1 inhibits influenza virus replication and improves severe influenza. *Cell* **153**, 112–125 (2013).
18. van den Pol, A. N. et al. Neuromedin B and gastrin-releasing peptide excite arcuate nucleus neuropeptide Y neurons in a novel transgenic mouse expressing strong Renilla green fluorescent protein in NPY neurons. *J. Neurosci.* **29**, 4622–4639 (2009).

19. Kuroda, E. et al. Inhaled fine particles induce alveolar macrophage death and interleukin-1α release to promote inducible bronchus-associated lymphoid tissue formation. *Immunity* **45**, 1299–1310 (2016).
20. Misharin, A. V., Morales-Nebreda, L., Mutlu, G. M., Budinger, G. R. & Perlman, H. Flow cytometric analysis of macrophages and dendritic cell subsets in the mouse lung. *Am. J. Respir. Cell Mol. Biol.* **49**, 503–510 (2013).
21. Zaynagetdinov, R. et al. Identification of myeloid cell subsets in murine lungs using flow cytometry. *Am. J. Respir. Cell Mol. Biol.* **49**, 180–189 (2013).
22. Weirauch, M. T. et al. Determination and inference of eukaryotic transcription factor sequence specificity. *Cell* **158**, 1431–1443 (2014).
23. Kostrzewa, R. M. & Jacobowitz, D. M. Pharmacological actions of 6-hydroxydopamine. *Pharmacol. Rev.* **26**, 199–288 (1974).
24. Cline, T. D., Beck, D. & Bianchini, E. Influenza virus replication in macrophages: balancing protection and pathogenesis. *J. Gen. Virol.* **98**, 2401–2412 (2017).
25. White, M. R. et al. Collectins, H-ficolin and LL-37 reduce influence viral replication in human monocytes and modulate virus-induced cytokine production. *Innate Immun.* **23**, 77–88 (2017).
26. Dimitrijevic, M., Stanojevic, S., Vujic, V., Beck-Sickinger, A. & von Horsten, S. Neuropeptide Y and its receptor subtypes specifically modulate rat peritoneal macrophage functions in vitro: counter regulation through Y1 and Y2/5 receptors. *Regul. Pept.* **124**, 163–172 (2005).
27. Wheway, J. et al. A fundamental bimodal role for neuropeptide Y1 receptor in the immune system. *J. Exp. Med.* **202**, 1527–1538 (2005).
28. Clausen, B. E., Burkhardt, C., Reith, W., Renkawitz, R. & Forster, I. Conditional gene targeting in macrophages and granulocytes using LysMcre mice. *Transgenic Res.* **8**, 265–277 (1999).
29. Pauli, E. K. et al. Influenza A virus inhibits type I IFN signaling via NF-κ B-dependent induction of SOCS-3 expression. *PLoS Pathog.* **4**, e1000196 (2008).
30. Bode, J. G. et al. IFN-α antagonistic activity of HCV core protein involves induction of suppressor of cytokine signaling-3. *FASEB J.* **17**, 488–490 (2003).
31. Moore, E. C., Barber, J. & Tripp, R. A. Respiratory syncytial virus (RSV) attachment and nonstructural proteins modify the type I interferon response associated with suppressor of cytokine signaling (SOCS) proteins and IFN-stimulated gene-15 (ISG15). *Virol. J.* **5**, 116 (2008).
32. Akhtar, L. N. et al. Suppressor of cytokine signaling 3 inhibits antiviral IFN-beta signaling to enhance HIV-1 replication in macrophages. *J. Immunol.* **185**, 2393–2404 (2010).
33. Kortlever, R. M. et al. Myc cooperates with ras by programming inflammation and immune suppression. *Cell* **171**, 1301–1315 (2017).
34. Londhe, V. A. et al. CXCR2 is critical for dsRNA-induced lung injury: relevance to viral lung infection. *J. Inflamm.* **2**, 4 (2005).
35. Li, S. et al. Epithelium-generated neuropeptide Y induces smooth muscle contraction to promote airway hyperresponsiveness. *J. Clin. Invest.* **126**, 1978–1982 (2016).
36. Lu, Y. & Ho, R. C. An association between neuropeptide Y levels and leukocyte subsets in stress-exacerbated asthmatic mice. *Neuropeptides* **57**, 53–58 (2016).
37. Singer, K. et al. Neuropeptide Y is produced by adipose tissue macrophages and regulates obesity-induced inflammation. *PLoS ONE* **8**, e57929 (2013).
38. Yasukawa, H. et al. IL-6 induces an anti-inflammatory response in the absence of SOCS3 in macrophages. *Nat. Immunol.* **4**, 551–556 (2003).
39. Zaloudikova, M. et al. Depletion of alveolar macrophages attenuates hypoxic pulmonary hypertension but not hypoxia-induced increase in serum concentration of MCP-1. *Physiol. Res.* **65**, 763–768 (2016).
40. Grebe, K. M. et al. Cutting edge: sympathetic nervous system increases proinflammatory cytokines and exacerbates influenza A virus pathogenesis. *J. Immunol.* **184**, 540–544 (2010).
41. Daidoji, T. et al. H5N1 avian influenza virus induces apoptotic cell death in mammalian airway epithelial cells. *J. Virol.* **82**, 11294–11307 (2008).
42. Imai, Y. et al. Identification of oxidative stress and Toll-like receptor 4 signaling as a key pathway of acute lung injury. *Cell* **133**, 235–249 (2008).
43. Imai, Y. et al. Angiotensin-converting enzyme 2 protects from severe acute lung failure. *Nature* **436**, 112–116 (2005).
44. Belperio, J. A. et al. Critical role for CXCR2 and CXCR2 ligands during the pathogenesis of ventilator-induced lung injury. *J. Clin. Invest.* **110**, 1703–1716 (2002).
45. Lu, Y. et al. Loss of *SOCS3* gene expression converts STAT3 function from anti-apoptotic to pro-apoptotic. *J. Biol. Chem.* **281**, 36683–36690 (2006).
46. Kim, D., Langmead, B. & Salzberg, S. L. HISAT: a fast spliced aligner with low memory requirements. *Nat. Methods* **12**, 357–360 (2015).
47. Liao, Y., Smyth, G. K. & Shi, W. featureCounts: an efficient general purpose program for assigning sequence reads to genomic features. *Bioinformatics* **30**, 923–930 (2014).
48. Robinson, M. D., McCarthy, D. J. & Smyth, G. K. edgeR: a Bioconductor package for differential expression analysis of digital gene expression data. *Bioinformatics* **26**, 139–140 (2010).
49. Zambelli, F., Pesole, G. & Pavesi, G. Pscan: finding over-represented transcription factor binding site motifs in sequences from co-regulated or co-expressed genes. *Nucleic Acids Res.* **37**, W247–W252 (2009).

Acknowledgements

The authors thank all members of their laboratories for helpful discussions. Y.Imai is supported by JSPS KAKENHI (S) grants 17H06179, 17K19693 and 15H05978. M.O. is supported by JSPS KAKENHI grant 17H06302. A.Y. is supported by JSPS KAKENHI grants 17H06175 and 18H05376, and AMED-CREST grants 18gm1110009 and 18gm0510019. K.K. is supported by JSPS KAKENHI grants 30733422, 16K19013, 17H04028 and JST PRESTO grant JPMJPR13MD. H.O. is supported by the Core Research for Evolutional Science and Technology (JPMJCR14W3-CREST). Y.Imai is supported by the Takeda Science Foundation and the Uehara Memorial Foundation. The authors acknowledge the NGS core facility of the Genome Information Research Center at the Research Institute for Microbial Diseases of Osaka University for their support with RNA-seq.

Author contributions

K.K., S.U., A.S.S., J.M.P., A.Y., H.O., H.H. and Y.Imai conceived the study and designed the experiments. S.F., M.H., Y.Ichida, D.L., E.K., K.J.I., H.T., M.G., H.I., R.H. and H.O. performed the experiments. S.M., M.O. Y.Ichida, and Y.Imai analysed the data. Y.Imai and H.H. wrote the manuscript with input from all authors.

Competing interests

The authors declare no competing interests.

Additional information

Supplementary information is available for this paper at https://doi.org/10.1038/s41564-018-0289-1.

Reprints and permissions information is available at www.nature.com/reprints.

Correspondence and requests for materials should be addressed to Y.I.

Publisher's note: Springer Nature remains neutral with regard to jurisdictional claims in published maps and institutional affiliations.

© The Author(s), under exclusive licence to Springer Nature Limited 2018

nature research

Corresponding author(s): Yumiko Imai

Life Sciences Reporting Summary

Nature Research wishes to improve the reproducibility of the work that we publish. This form is intended for publication with all accepted life science papers and provides structure for consistency and transparency in reporting. Every life science submission will use this form; some list items might not apply to an individual manuscript, but all fields must be completed for clarity.

For further information on the points included in this form, see Reporting Life Sciences Research. For further information on Nature Research policies, including our data availability policy, see Authors & Referees and the Editorial Policy Checklist.

Please do not complete any field with "not applicable" or n/a. Refer to the help text for what text to use if an item is not relevant to your study.

For final submission: please carefully check your responses for accuracy; you will not be able to make changes later.

Experimental design

1. Sample size

Describe how sample size was determined.

We did not predetermine sample size. All experiments were performed multiple times and conclusions were considered valid if results were reproducible between experiments.

2. Data exclusions

Describe any data exclusions.

We excluded the data using outlier calculator by GraphPad software (https://www.graphpad.com/quickcalcs/grubbs1/).

3. Replication

Describe the measures taken to verify the reproducibility of the experimental findings.

All attempts at replication were successful.

4. Randomization

Describe how samples/organisms/participants were allocated into experimental groups.

Samples were not allocated into experimental group in random. Mice were chosen based on their genotype, age, and sex.

5. Blinding

Describe whether the investigators were blinded to group allocation during data collection and/or analysis.

The investigators were blinded to group allocation during data collection and analysis.

Note: all in vivo studies must report how sample size was determined and whether blinding and randomization were used.

6. Statistical parameters

For all figures and tables that use statistical methods, confirm that the following items are present in relevant figure legends (or in the Methods section if additional space is needed).

n/a	Confirmed	
☐	☒	The exact sample size (*n*) for each experimental group/condition, given as a discrete number and unit of measurement (animals, litters, cultures, etc.)
☐	☒	A description of how samples were collected, noting whether measurements were taken from distinct samples or whether the same sample was measured repeatedly
☐	☒	A statement indicating how many times each experiment was replicated
☐	☒	The statistical test(s) used and whether they are one- or two-sided *Only common tests should be described solely by name; describe more complex techniques in the Methods section.*
☐	☒	A description of any assumptions or corrections, such as an adjustment for multiple comparisons
☐	☒	Test values indicating whether an effect is present *Provide confidence intervals or give results of significance tests (e.g. P values) as exact values whenever appropriate and with effect sizes noted.*
☐	☒	A clear description of statistics including central tendency (e.g. median, mean) and variation (e.g. standard deviation, interquartile range)
☐	☒	Clearly defined error bars in all relevant figure captions (with explicit mention of central tendency and variation)

See the web collection on statistics for biologists for further resources and guidance.

Software

Policy information about availability of computer code

7. Software

Describe the software used to analyze the data in this study.	Data were analyzed using Graphpad Prism 5 or 6 (graphing, statistical analysis) , and BD Accuri C6 software (flow cytometry).

For manuscripts utilizing custom algorithms or software that are central to the paper but not yet described in the published literature, software must be made available to editors and reviewers upon request. We strongly encourage code deposition in a community repository (e.g. GitHub). *Nature Methods* guidance for providing algorithms and software for publication provides further information on this topic.

Materials and reagents

Policy information about availability of materials

8. Materials availability

Indicate whether there are restrictions on availability of unique materials or if these materials are only available for distribution by a third party.	Materials are available upon request.

9. Antibodies

Describe the antibodies used and how they were validated for use in the system under study (i.e. assay and species).	All antibodies except one used for FFU assay were commercially available as below, and used only on species for which they have been validated by the vendor. Mouse monoclonal anti-GFP (clone 1E4) MBL M048-3 Rabbit polyclonal anti-Tyrosine hydroxylase Millipore AB152 Rabbit polyclonal anti-Y1R SantaCruz sc-28949 Rabbit polyclonal anti-Y2R Neuromics RA14136 Rat monoclonal anti-CD11b-PE (clone M1/70) eBioscience 12-0112-81 Hamster monoclonal anti-CD11c-PE (clone HL3) BD 557401 Rat monoclonal anti-Ly6-C-PE (clone HK1.4) Biolegend 128007 Rat monoclonal anti-Ly6-G-PE (clone 1A8) Biolegend 127607 Rat monoclonal anti-Siglec-F-PE (clone E50-2440) BD 552126 Hamster monoclonal anti-CD103-PE (clone 2E7) eBioscience 2-1031-82 Mouse monoclonal anti-CD3-PE (clone eBioG4.18) eBioscience 12-0041-82 Mouse monoclonal anti-NK1.1-PE (clone PK136) Biolegend 108707 Goat polyclonalanti- GFP Abcam ab5450 Rabbit polyclonal anti-SOCS3 IBL 18395 Rabbit monoclonal anti-phospho-STAT3 (Tyr705)(clone D3A7) CST 9145 Rabbit monoclonal anti-STAT3 (clone D3Z2G) CST 12640 Rabbit monoclonal anti-GAPDH (clone 14C10) CST 2118 Rat monoclonal anti-CD11b-PerCP-Cy5.5 (clone M1/70) BD 550993 Mouse monoclonal anti-CD11b-APC (clone ICRF44) TONBO biosciences 20-0118-T025 Rat monoclonal anti-Siglec-F-PerCP-eFluor 710 (clone 1RNM44N) eBioscience 46-1702-80 Rat monoclonal anti-F4/80-PE (clone BM8) Biolegend 123110 Rat monoclonal anti-F4/80-APC (clone BM8) eBioscience 17-4801-82 For FFU assay, we used Ab that reacts with common sequences of the influenza virus nucleoprotein (NP) and matrix protein 1 (M1) (reference 53). This Ab was validated and provided by Dr. Nakaya.

10. Eukaryotic cell lines

a. State the source of each eukaryotic cell line used.	WT and SOCS3 KO MEFs (reference 57) were provided by Dr. Yoshimura.
b. Describe the method of cell line authentication used.	Cell lines were not authenticated in our laboratory.
c. Report whether the cell lines were tested for mycoplasma contamination.	All cell lines tested negative for mycoplasma contamination.
d. If any of the cell lines used are listed in the database of commonly misidentified cell lines maintained by ICLAC, provide a scientific rationale for their use.	No commonly misidentified cell lines were used.

Animals and human research participants

Policy information about studies involving animals; when reporting animal research, follow the ARRIVE guidelines

11. Description of research animals

Provide all relevant details on animals and/or animal-derived materials used in the study.

NPY-KO, NPY-GFP and Lysozyme Cre mice were obtained from Jackson laboratory (reference 35). Background of NPY-KO mice are 129/SvJ. 129/SvJ mice were bred at our animal facility. Y1R-floxed(reference34), SOCS3-floxed mice (reference51) were generated as previously described. Y1R-floxed and SOCS3-floxed mice were crossed with Lysozyme Cre recombinase strain (reference35) to generate myeloid cell-specific Y1R and SOCS3 knockout mice, respectively.

Policy information about studies involving human research participants

12. Description of human research participants

Describe the covariate-relevant population characteristics of the human research participants.

The study did not involve human research participants.